Separation Science and Technology

ISSN: 0149-6395 (Print) 1520-5754 (Online) Journal homepage: https://www.tandfonline.com/loi/lsst20

Modeling of Particle Fouling and Membrane Blocking in Submerged Membrane Filtration

Kuo-Jen Hwang & Fung-Fu Chen

To cite this article: Kuo-Jen Hwang & Fung-Fu Chen (2007) Modeling of Particle Fouling and Membrane Blocking in Submerged Membrane Filtration, Separation Science and Technology, 42:12, 2595-2614, DOI: 10.1080/01496390701513081

To link to this article: https://doi.org/10.1080/01496390701513081

Published online: 02 Oct 2007.

Separation Science and Technology, 42: 2595–2614, 2007

ISSN 0149-6395 print/1520-5754 online
DOI: 10.1080/01496390701513081

Modeling of Particle Fouling and Membrane Blocking in Submerged Membrane Filtration

Kuo-Jen Hwang and Fung-Fu Chen
Department of Chemical and Materials Engineering, Tamkang University, Tamsui, Taipei Hsien, Taiwan

Abstract: The models of particle fouling and membrane blocking in a submerged membrane filtration are developed in this study. The effects of operating conditions, such as aeration intensity (air flow rate) and filtration pressure, on the filtration flux, membrane blocking, and cake formation are discussed thoroughly. The experimental results show that the filtration resistances due to cake formation and membrane blocking play significant roles in determining the overall filtration resistance, but the latter one is more dominant. An increase in aeration intensity leads the filtration flux to increase due to the reduction of cake formation on the membrane surface. However, a higher filtration pressure causes more severe membrane internal blocking and then to lower filtration flux. The cake properties and the filtration resistance due to membrane blocking are analyzed and can be regressed to empirical functions of filtration pressure. A force balance model for particle deposition on the membrane surface is also derived. In order to estimate the shear stress acting on the membrane surface, the diameter, shape, and rising velocity of air bubbles are analyzed based on hydrodynamics. Once the model coefficients are obtained, the pseudo-steady filtration flux under various conditions can be estimated by the proposed model and the basic filtration equation. The calculated results agree fairly well with the available experimental data.

Keywords: Membrane filtration, particle fouling, microfiltration, particle deposition, cake properties

Received 20 December 2006, Accepted 17 April 2007
Address correspondence to Kuo-Jen Hwang, Department of Chemical and Materials Engineering, Tamkang University, Tamsui, Taipei Hsien 25137, Taiwan. Fax: +886-2-26209887; E-mail: kjhwang@mail.tku.edu.tw

INTRODUCTION

A submerged membrane bioreactor has a potential to be applied to wastewater treatments in recent years. In an aerobic membrane bioreactor, the uplifting air-bubble flow plays the roles of oxygen supply for microbial cells and cake removal. Although it has many advantages compared to those conventional wastewater treatment processes, some operating characteristics, such as membrane fouling and the oxygen transfer of biological suspension, become the main barrier to faster development of this process. Therefore, to understand the particle fouling in an aerated membrane filtration is one of the main gateways to developing an efficient membrane bioreactor system.

Hydrodynamic and microbial conditions are major factors affecting the performance of a membrane bioreactor. The impacts of aeration rate, sludge concentration, membrane diameter, and membrane length on the membrane flux and particle fouling have been discussed experimentally in several previous studies (1–9). However, none of those studies drew a quantitative or theoretical correlation between the membrane fouling and hydrodynamic conditions, which restricted the application of their experimental results. Recently, Liu et al. (10) proposed an empirical relationship among the permeating flux, hydrodynamic conditions, and sludge concentration. Prior to employing the equation, the used parameters should be regressed from experimental data.

In practice, a little information was available on the hydrodynamic analysis of biosolids during submerged membrane filtration in bioreactors. Choo and Lee (11) investigated the hydrodynamic behavior of biosolids on membrane filterability based on a theoretical approach of biosolids transport. The flux decline was evaluated in terms of hydraulic resistances, biosolid sizes, and operating conditions. They concluded that the permeate flux was mainly dependent on the biosolid build-up on the membrane surface, especially under low sludge age conditions. However, the roles of colloidal and soluble components were also important because of causing the pore blocking or irreversible fouling. Lee et al. (12) reported that the membrane resistance, cake resistance, blocking, or irreversible fouling resistance in a submerged membrane bioreactor contributed 12%, 80%, and 8%, respectively, to the overall filtration resistance. Bouhabila et al. (4, 13) observed that the supernatant of MLSS had 20–30 times higher specific resistance than the sludge suspension, which illustrated the high fouling potential of soluble and colloidal fractions.

When particle fouling occurs in a membrane filtration, particles deposit on or migrate into the membrane pores causing the filtration flux to decline quickly. Several remedial methods have been proposed to prevent or reduce the membrane fouling, such as increasing fluid velocity, backwashing, sparging air bubbles, or introducing turbulent flow, etc. (14). In a submerged membrane filtration system, the membrane fouling is significantly

determined by the aeration intensity and bubble flow pattern (9, 15). Although increasing the aeration intensity or increasing the bubble flow rate is commonly believed to be helpful for reducing particle fouling, optimum aeration intensity should be carefully determined for economic and efficient consideration. Therefore, to understand the relationships among aeration intensity, particle fouling and filtration flux becomes an essential step for achieving optimum system design.

In recent years, several models have been proposed for understanding the particle fouling or predicting the pseudo-steady filtration flux in microfiltration. When macromolecules or colloids were filtered, the diffusion mass transport phenomenon was dominant, and the concentration polarization models were commonly used for predicting the concentration profile near the membrane surface as well as the pseudo-steady filtration flux (16). When a filter cake formed on the membrane played the major role on the overall filtration resistance, the hydrodynamic models were frequently adopted for explaining the particle deposition and flux attenuation (14, 17). The stability of the particles staying on the membrane surface could be analyzed by a force balance model (18) or a moment balance model (19). Besides, the membrane blocking models were employed to analyze how and when the membrane pores were blocked by fine particles when the size of the particles was smaller than those of the membrane pores (18, 20, 21).

As mentioned previously, the hydrodynamic conditions are of significance for retarding membrane fouling and maintaining stable permeating flux in submerged membrane filtration. In this study, a typical particulate sample is used for modeling the suspended solids in membrane bioreactors. The effects of operating conditions, such as aeration intensity and filtration pressure, on the filtration flux, particle fouling, filtration resistances, and cake properties are discussed. A hydrodynamic model is also derived for calculating the shear stress acting on the membrane surface and the critical condition for particle deposition.

FORCE BALANCE MODEL FOR PARTICLE DEPOSITION

A schematic diagram of the filtration system near the membrane surface is shown in Fig. 1. Some particles are transported to arrive at the filter membrane due to the filtrate flow during a filtration. A few particles may migrate into the membrane pores to block the pores; in contrast, some of the other particles can deposit stably on the membrane surface when the friction force exceeds the tangential force exerted on the particles. Refer to the enlarged figure shown in Fig. 1, the forces exerted on a depositing particle include the drag forces in the tangential and filtration directions, respectively, and the net gravitational force. Since the net up-flow velocity of particles is very small and the particle size is larger than 1 μm, the

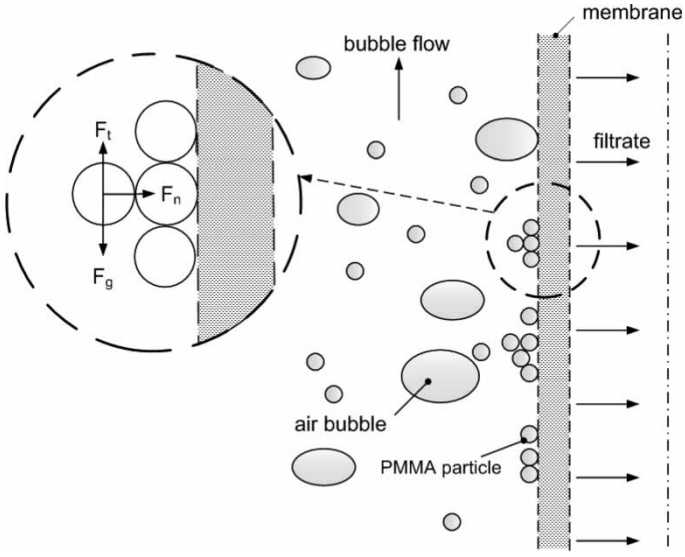

Figure 1. Force analysis for a depositing particle.

inertial lift force and net interparticle force are commonly much smaller than the drag forces and can be neglected reasonably. Hence, the force balance model at the pseudo-steady condition, at which the particle can just deposit stably, can be simplified to (17, 18):

$$(F_t - F_g) = f_c F_n, \tag{1}$$

where f_c is the friction coefficient between particles, while F_t, F_n, and F_g are the drag forces in the tangential and filtration directions, respectively, and the net gravitational force. According to Eq. (1), if the net tangential force $(F_t - F_g)$ exceeds the friction force $(f_c F_n)$, the particle will be swept away from its original position and be transported back to the bulk suspension. Otherwise, the particle can deposit stably.

Based on the analysis of Hwang and Lin (18), the tangential drag force can be estimated by the modified Stokes law because of the low Reynolds number tangential flow near the membrane surface, that is,

$$F_t = C_1 d_p^2 \tau_w, \tag{2}$$

where d_p is the particle diameter, τ_w is the shear stress acting on the membrane surface, and C_1 is a correction factor for the existences of the filter cake and the membrane. The actual shear stress generated by rising bubbles is very hard to analyze, but it can be considered to be proportional to the shear stress acting on the surface of the rising bubbles, τ_b, and the bubble generation

frequency, f_r. Introducing the drag coefficient, C_D, the shear stress acting on bubble surface can be calculated by

$$\tau_b = C_D \cdot \left(\frac{\rho_b \cdot u_b^2}{2} \right) \tag{3}$$

where ρ_b and u_b are the density and rising velocity of the bubble, respectively. For a single air bubble of negligible density, the drag coefficient is commonly defined as (22):

$$C_D \equiv \frac{4 g d_b}{3 u_b^2} \tag{4}$$

Therefore, the shear stress acting on the membrane surface can be estimated by the following equation:

$$\tau_w = C_2 \, \tau_b \cdot f_r = C_2 \times \frac{2 \rho_b \, g \, d_b}{3} f_r \tag{5}$$

Since the bubble frequency is proportional to the aeration intensity, it can be calculated by

$$f_r = \frac{Q}{V_b} = \frac{6 \, Q}{\pi \, d_b^3} \tag{6}$$

where Q is the air volumetric flow rate, V_b and d_b are the volume and equivalent diameter of a single bubble, respectively. The relationship between d_b and Q can be measured in experiments or directly obtained by the dimensional analysis (22).

Substitution of Eqs. (5) and (6) into Eq. (2), the tangential drag force can be estimated by the following equation:

$$F_t = C_1 \, C_2 \, d_p^2 \cdot \tau_b \cdot f_r = C_3 \frac{\rho_b \, d_p^2 \, Q}{d_b^2} \tag{7}$$

Therefore, the tangential drag force on the particles in a specified suspension is mainly dependent on the aeration intensity and bubble size.

The net gravitational force on the particle can be calculated by

$$F_g = \frac{\pi \, d_p^3 (\rho_p - \rho_l) \, g}{6} \tag{8}$$

where ρ_p and ρ_l are the densities of particle and liquid, respectively.

The normal drag can also be calculated by the modified Stokes law since the Reynolds number in the filtration direction is very low in most conditions, i.e.,

$$F_n = 3 \pi \mu d_p q_s C_4 \tag{9}$$

where μ is the liquid viscosity, while q_s is the pseudo-steady flux. The correction factor, C_4, is due to the existence of the cake and the membrane. Since the

thickness of the cake and the membrane are far larger than the particle diameter, the results of Sherwood (23) for a thick porous medium can be employed for evaluated C_4, that is,

$$C_4 = 0.36(R_t\, d_p^2/4L_m)^{2/5} \tag{10}$$

where L_m is the thickness of the porous medium. The porous medium should take both the membrane and cake into consideration.

After substituting Eqs. (7)–(9) into Eq. (1), the pseudo-steady flux and cake thickness are the two residual unknowns except for operating conditions and coefficients yet to be determined.

Furthermore, the basic filtration equation can be written as:

$$q = \frac{\Delta P}{\mu R_t} = \frac{\Delta P}{\mu(R_c + R_{if} + R_m)} \tag{11}$$

The overall filtration resistance, R_t, can be obtained by summing the filtration resistances due to the filter cake, R_c, to the membrane internal fouling, R_{if}, and to the clean membrane, R_m. The cake resistance can be given by

$$R_c = w_c\, \alpha_{av}, \tag{12}$$

in which w_c and α_{av} are the mass and average specific filtration resistance of cake, respectively. Based on a material balance, the cake mass can be calculated by

$$w_c = \rho_p(1 - \varepsilon_{av})\, L_c \tag{13}$$

where ε_{av} is the average cake porosity and L_c is the cake thickness. If the cake thickness and cake mass can be measured in experiments, the value of ε_{av} and α_{av} can then be estimated accordingly. Hence, α_{av} and ε_{av} can be expressed as power functions of the filtration pressure according to Tiller's empirical equations (24). Once the filtration resistances are related to filtration pressure and bubble flow pattern, the residual unknowns in Eq. (11) are also filtration flux and cake thickness. Therefore, the pseudo-steady filtration flux and cake thickness can be estimated by solving Eq. (1) and Eq. (11) simultaneously.

MATERIALS AND METHODS

A kind of spherical particles made of polymethly methacrylate (PMMA) was used as a typical particulate sample in experiments. The particles with a catalog number of MX-500 were manufactured by Soken Co. in Japan. The particle size distribution was very narrow. The mean diameter and density of the particles were 5.0 μm and 1190 kg/m^3, respectively. The particles were suspended in de-ionized water to prepare a 0.1 wt% suspension. The pH value and the temperature of the suspension were kept at 7.0 and 20°C, respectively, during filtration. The zeta potential of particles was measured

as -20 mV using a zeta sizer of Malvern 4700. A hydrophilic ceramic membrane (# Kerasep 06040) manufactured by Orelis Co. in France was used in the experiments as the filter medium. The cylindrical membrane was made of ZrO_2-TiO_2 and had an inner diameter of 6.0×10^{-3} m, an outer diameter of 1.0×10^{-2} m, and a length of 4.0×10^{-1} m. Its pore size distribution on the outer membrane surface ranged from 1 to 20 μm and is shown in Fig. 2.

A schematic diagram of the cross-flow microfiltration system used in this study is shown in Fig. 3. Before each experiment, the particles were suspended uniformly in the 80-liter suspension tank using a mechanical mixer. Air bubbles were introduced by a diffuser which installed under the membrane, and the bubble flow rate was adjusted and measured by a rotameter. The filtration pressure was supplied by a vacuum pump and was adjusted carefully to a set value by the regulator. Any increase in the filtrate weight during filtration could be detected by the load cell and recorded via a personal computer. The size, shape, and frequency of the air-bubbles in the filtration system could be detected and recorded by a video recorder through the transparent wall of the suspension tank. When the experiment was terminated, the cake formed on the filter membrane was measured its thickness by a vernier from the photograph taking by a digital camera and sent to analyze its wet and dry masses by an *ORION* AD-4714A moisture titrator.

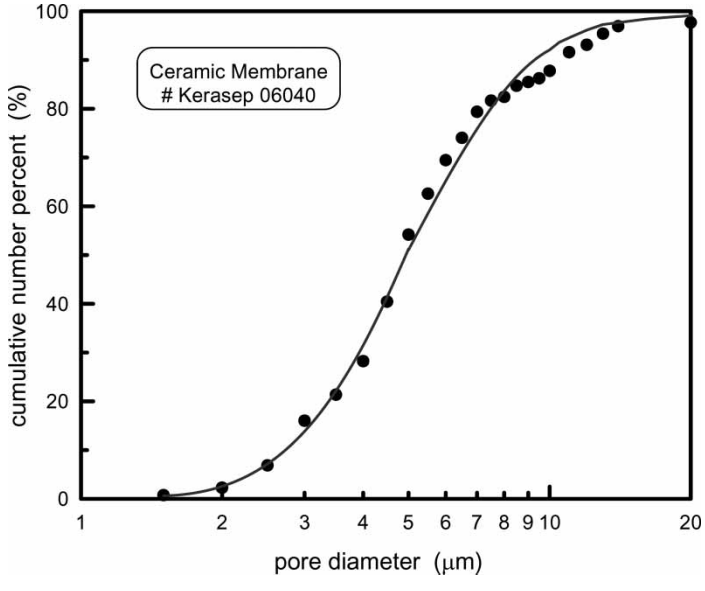

Figure 2. The pore size distribution on the membrane outer surface.

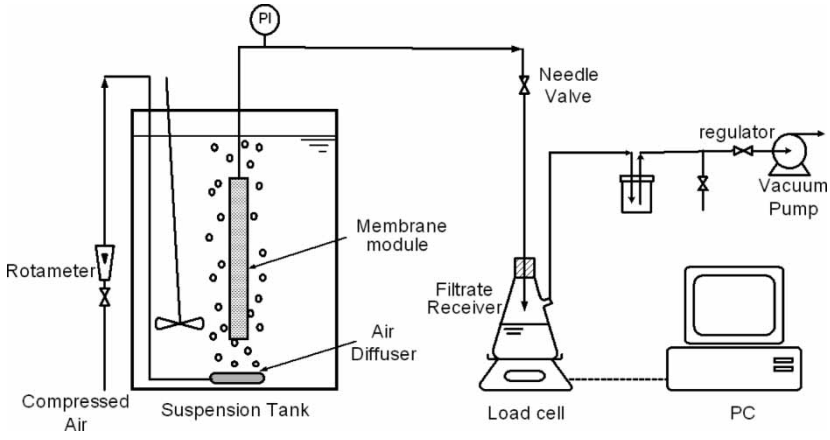

Figure 3. A schematic diagram of the submerged membrane filtration system.

RESULTS AND DISCUSSION

Figure 4 shows the time courses of filtration flux in submerged membrane filtration under various filtration pressures and no any aeration. At the beginning of filtration, the filtration flux attenuates very quickly due to the particle fouling. However, the flux gradually approaches a pseudo-steady value after

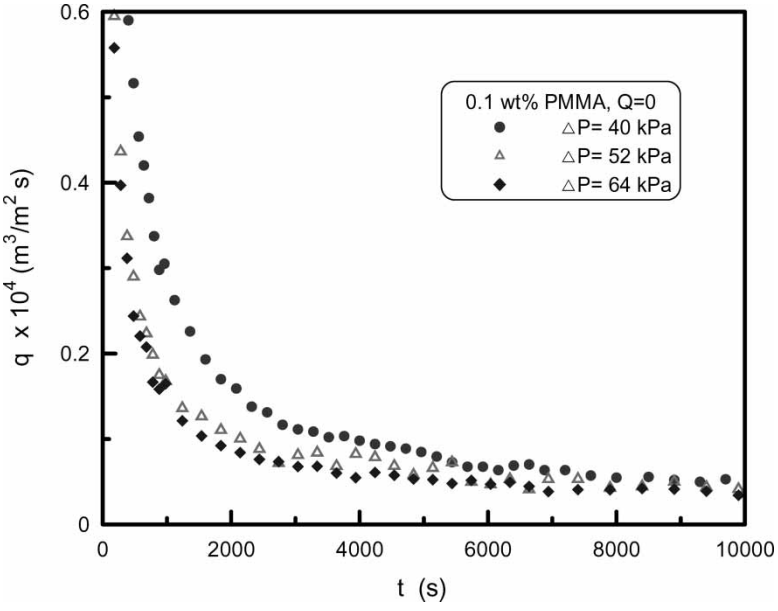

Figure 4. The time courses of filtration flux during microfiltration under different filtration pressures and none aeration.

3000 s. Although the trend of the curves is similar to those in previous studies (17, 18), the filtration pressure plays an opposite role on the filtration flux. An increase in filtration pressure leads to a lower flux. This may be due to more considerable cake formation or more severe membrane internal blocking under a higher pressure. The unexpected increase in filtration resistance causes the filtration flux to decrease. The phenomena will be well-discussed later. In fact, the condition of no aeration provides a convenient way to calculate the friction factor between particles, f_c. According to the force balance model, Eq. (1), the value of F_t is equal to zero under the condition of no aeration, and the values of F_g and F_n can be calculated by solving Eqs. (8) and (9), respectively. Hence, the value of f_c is the only residue unknown in Eq. (1) and can then be easily solved. The value of f_c for the PMMA particles used in this study is calculated as 0.03.

The size, shape, and rising velocity of bubbles are important factors to affect the shear stress acting on the membrane surface. In the previous study (22), dimensional analysis was employed to study the bubble flow system, and three important dimensionless groups, Reynolds number (Re$_b$), Morton number (*Mo*), and Eotvos number (*Eo*), were obtained. According to the observation on air bubble flow in the system shown in Fig. 3 and the results of dimensional analysis (22), the air bubbles are in oblate ellipsoidal shape within the operating conditions in this study. Figure 5 shows the effect of air volumetric flow rate on the bubble size and rising velocity. The

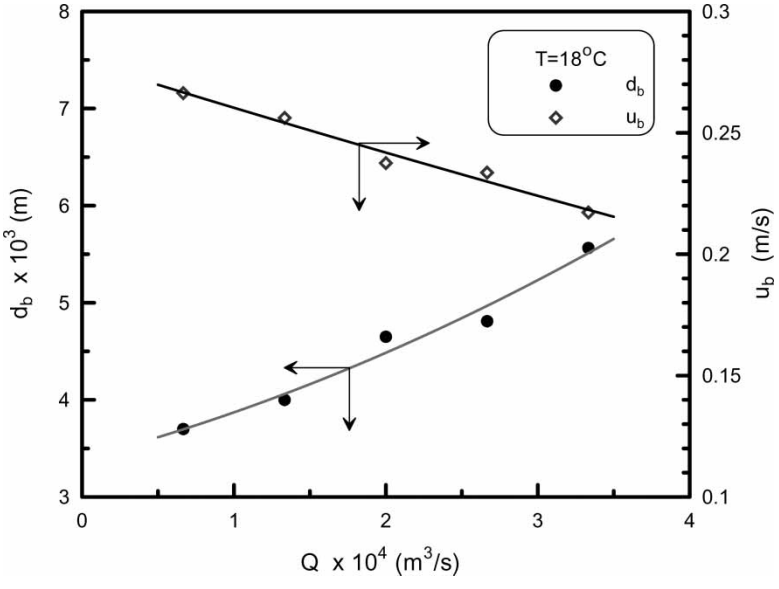

Figure 5. The equivalent diameter and velocity of the raising air bubbles under various aeration intensities.

bubble image is captured by a video recorder and analyzed by a Power Image Analysis System, and the data are converted to equivalent diameters. Once the bubble size is known, the rising velocity of air bubbles can be estimated by empirical equations (25), e.g.,

$$u_b = 1.35\left(\frac{2\sigma}{\rho_l d_b}\right)^{0.5} \text{ when } 4.02Mo^{-0.214} < \text{Re}_b \leq 3.10Mo^{-0.25} \quad (14)$$

and

$$u_b = 1.53\left(\frac{\sigma g}{\rho_l}\right)^{0.25} \text{ when } 3.10Mo^{-0.25} < \text{Re}_b \quad (15)$$

where σ is the surface tension. An increase in the air flow rate leads to bigger bubbles but to a slower rising velocity, as shown in Fig. 5. The mean bubble diameters range from 3.5 to 5.5 mm, while the rising velocities range from 0.21 to 0.27 m/s under the conditions of this study. From a previous analysis of air bubble rising in stagnant water (25), the rising velocity for a single bubble decreases as the equivalent diameter of bubbles ranges from 2 to 5 mm. Under such conditions, the bubbles are flattened and rise in a zigzag pattern, with significantly increased drag coefficients. The bubble observations in this study agree fairly with these results.

The variation of filtration fluxes shown in Fig. 4 becomes trivial after 8,000 s; therefore, the pseudo-steady filtration flux is defined as the average flux between 8,000 and 10,000 s in this study. Figure 6 shows the effects of filtration pressure and air volumetric flow rate on the pseudo-steady filtration flux. Although the driving force is increased by increasing filtration pressure, a linear decrease in filtration flux can be obtained. This reveals that the particle fouling becomes more severe under a higher pressure. Since the increased extent in overall filtration resistance exceeds that of the driving force, increasing filtration pressure is not a proper method to enhance the filtration flux in this system. Moreover, the increase in air flow rate causes an increase in the filtration flux. A 1.2-fold increase in filtration flux can be obtained when the air flow rate increases from none to 3.33×10^{-4} m^3/s under a fixed filtration pressure of 40 kPa. This is because a higher air flow rate results in higher shear stress acting on the membrane surface as well as lower probability of particle fouling, which in tern helps enhancing the filtration flux.

In order to understand the mechanism of microfiltration using a submerged membrane, the filtration resistances from various sources are analyzed using the method described in the authors' previous study (26). The important filtration resistances in most microfiltration include the filtration resistances due to membrane internal fouling, R_{if}, due to clean membrane, R_m, and due to the filter cake, R_c. The overall filtration resistance, R_t, can be calculated from the filtration data by solving Eq. (11), while R_m from the pure water flux before filtration. When a filtration is terminated, the value of R_{if} can be

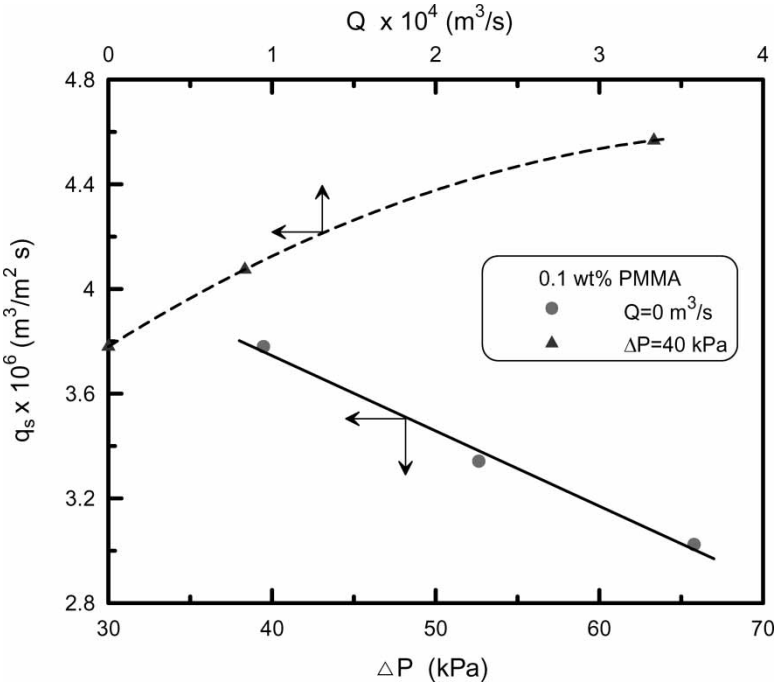

Figure 6. The pseudo-steady filtration fluxes under various aeration intensities and filtration pressures.

obtained from the difference between pure water flux before and after the membrane cleaning. The value of R_c can therefore be calculated by Eq. (11) once the other resistance are known. Figure 7 shows a comparison of these filtration resistances under various air flow rates and under a fixed filtration pressure of 40 kPa. No obvious effects of air flow rate on the values of R_{if} and R_m can be found in this figure. This reveals that the air bubble flow cannot prevent or affect the particle fouling occurring in the membrane pores. However, the cake resistance, R_c, decreases markedly as the air flow rate increases. This indicates that the extra shear stress generated by the air bubble flow can efficiently reduce the particle deposition on the membrane surface. A 75% decrease in cake resistance can be obtained as the air flow rate increases from 0 to 3.33×10^{-4} m^3/s. This fact results in a decrease in the overall filtration resistance, as shown in Fig. 7. Furthermore, 50–80% of the overall filtration resistance can be attributed to the membrane internal fouling within the operating conditions of this study. The values of R_c account for 10–30%, while R_m only for 2%, of the overall resistance. Since over 90% of filtration resistance is due to the particle fouling in and on the membrane, to reduce the particle fouling may efficiently enhance the filtration flux.

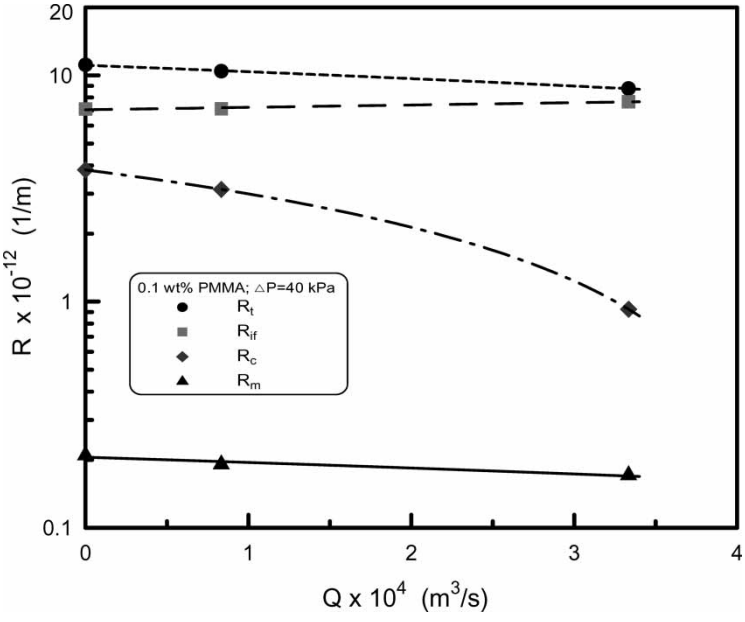

Figure 7. The filtration resistances under various aeration intensities and a fixed filtration pressure of 40 kPa.

The effects of operating conditions on the filtration resistance due to membrane internal fouling are shown in Fig. 8. Since a higher filtration pressure may lead particles to have more opportunity to penetrate into the membrane pores at the beginning of filtration, the value of R_{if} increases with increasing filtration pressure. Moreover, as indicated in Fig. 7, no obvious effect of air flow rate on R_{if} was found, this fact can also be seen in Fig. 8 even under the other filtration pressures. Therefore, filtration pressure becomes the sole effect on the value of R_{if}, and the relationship between R_{if} and ΔP can be regressed as:

$$R_{if} = 3.22 \times 10^{12} \exp(1.94 \times 10^{-5} \Delta P) \tag{16}$$

in which the unit of pressure is N/m^2. Consequently, the resistance due to membrane internal fouling under a specified filtration pressure can be estimated by employing the above exponential-type empirical equation. In short, as discussed in Fig. 6, increasing filtration pressure may not be an acceptable way for enhancing the filtration flux in this system because of the marked increase of R_{if}.

Figure 9 shows the effects of air flow rate and filtration pressure on the cake resistance. Since the flow of air bubbles reduces the cake formation on the membrane surface, an increase in air flow rate leads to lower cake resistance under a fixed filtration pressure. This trend is similar to those in

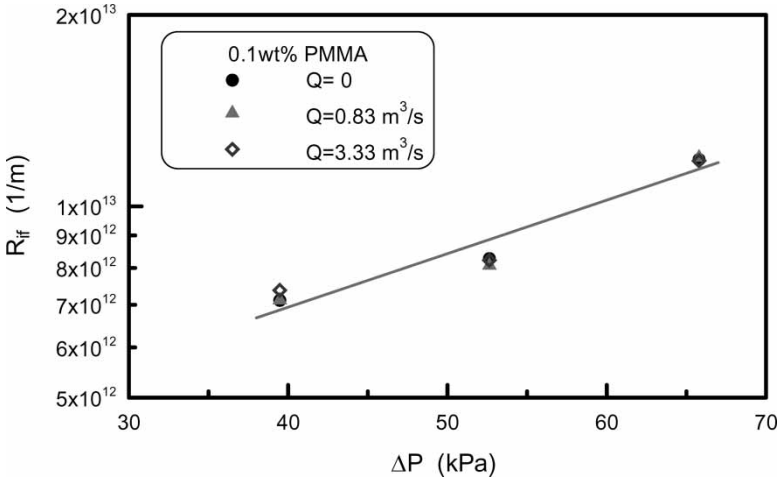

Figure 8. Filtration resistances due to membrane internal fouling under various aeration intensities and filtration pressures.

previous studies (9, 15), and the filtration flux is then increased by increasing aeration intensity, as shown in Fig. 6. Furthermore, the value of R_c increases with the increase of filtration pressure under a given air flow rate. This trend is the same as the results in most filtration (14, 16–19). A two to five-fold (depending on the air flow rate) increase in cake resistance can be found when the filtration pressure is increased 1.6-fold (from 40 to 64 kPa). Since

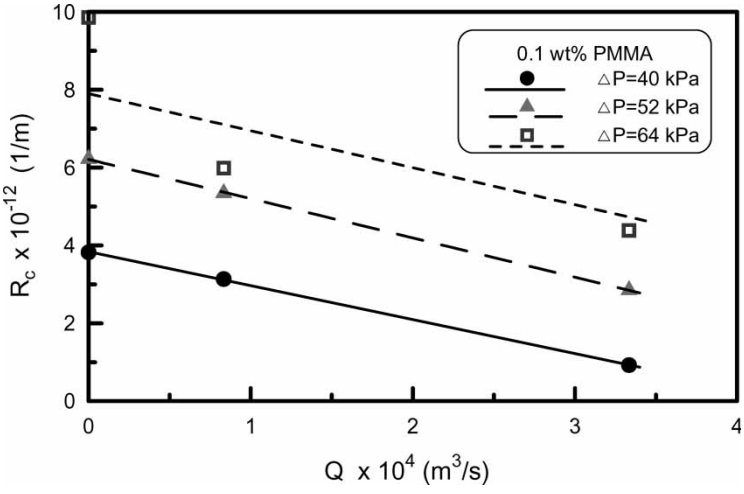

Figure 9. Effects of aeration intensity and filtration pressure on the cake filtration resistances.

the increasing extent of cake filtration resistance exceeds the increase in filtration driving force, increasing filtration pressure is adverse for the filtration performance. To consider all the results shown in Figs. 7–9, the filtration flux can be enhanced by increasing aeration intensity but be reduced by increasing filtration pressure. The curve trends shown in Figs. 4 and 6 can then be reasonably explained.

Based on the conventional filtration theory, the cake filtration resistance can be expressed as the product of the mass and average specific filtration resistance of cake, e.g., Eq. (12). Therefore, an analysis on these cake properties is helpful for understanding the effects of operating conditions on the cake filtration resistance. The experimental data of porosity and average specific filtration resistance of the cake are co-plotted against the filtration pressure in Fig. 10 in logarithmic scales. An increase in filtration pressure causes more cake compression, consequently, to higher specific filtration resistance and lower cake porosity. These tendencies are similar to those in most filtration (17, 24). Since the data can be regressed to straight lines as shown in Fig. 10, the Tiller's power-type empirical functions can be employed to correlate these cake properties and filtration pressure, and the index of cake compressibility can then be obtained from the slopes of the α_{av} vs. ΔP lines (24), that is as high as 1.1. To consider the data shown in Fig. 10, the cake porosity ranges from 0.4 to 0.45 in this study. Those compact cake structures cause the specific cake filtration resistance to be unusual high, e.g., an order of 10^{13} m/kg for 5 μm particles. Since no obvious effect of air flow rate on the cake properties can be found in the experimental results of this study, the data under the other aeration intensities are therefore not shown in the figure.

Figure 11 shows the masses of cakes constructed on the membrane surface under various air flow rates and filtration pressures. Just the same as

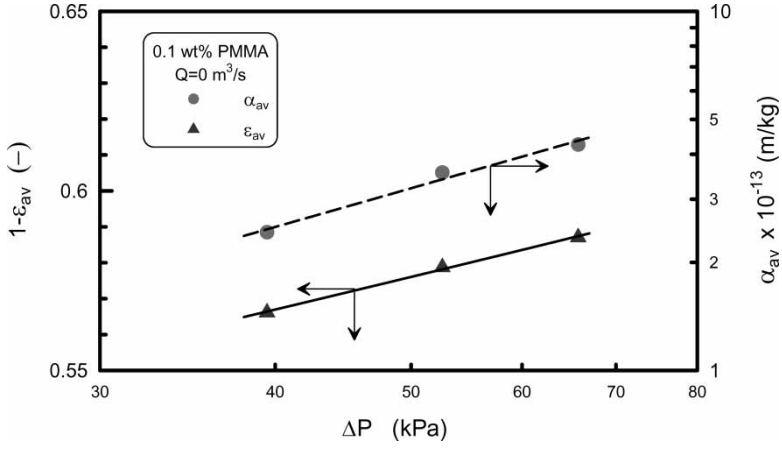

Figure 10. Effect of filtration pressure on the porosity and specific filtration resistance of cake.

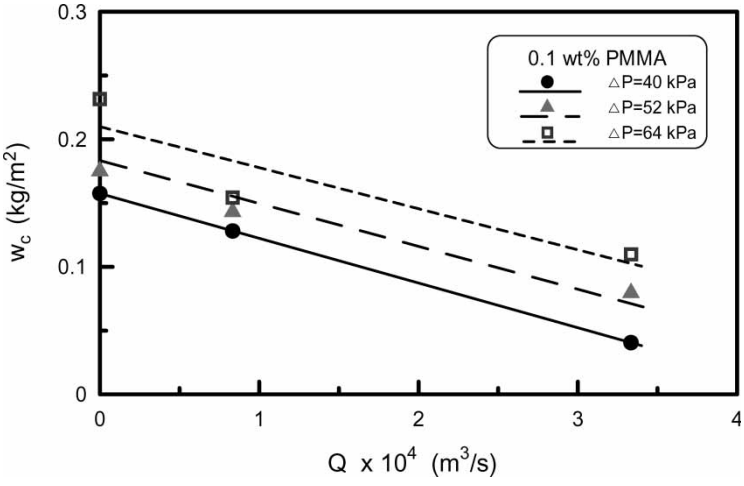

Figure 11. Effects of operating conditions on the cake mass.

previous discussions, the aeration can significantly reduce the cake formation on the membrane surface, i.e., the cake mass decreases with the increase of air flow rate. The data indicate that the cake mass formed under aeration is only 30–75% of that in the non-aeration condition, and that the cake mass is strongly dependent on the filtration pressure. This can be used to reasonably explain why the filtration flux can be enhanced by aeration. Furthermore, the cake mass also increases with increasing filtration pressure. It is because the particles staying on the membrane are more stable, or in other words, are more easily deposited under a higher filtration pressure (17, 18). Considering the results shown in Figs. 10 and 11, the cake filtration resistance is increased by increasing filtration pressure due to both the increases in cake mass and the specific filtration resistance.

According to the force analysis in this study, the tangential drag force acting on the membrane surface due to the rising bubbles is proportional to the term of $\rho_b d_p^2 Q/d_b^2$. Therefore, the other terms in Eq. (1), $(f_c F_n + F_g)$, under various conditions are plotted against $\rho_b d_p^2 Q/d_b^2$ in Fig. 12 in order to verify the correction of the force balance model for particle deposition. Although the data are obtained under different air flow rates and filtration pressures, a straight line can be regressed, as shown in Fig. 12. This result demonstrates the reliability of the proposed model, and the coefficient C_3 in Eq. (7) can then be given from the slope of the line. Moreover, an interesting phenomenon can also be seen in Fig. 12 that the straight line does pass through the origin; it has an intercept ca 2.44×10^{-13} N/m^2. The filtration system is similar to a "dead-end" cake filtration in the condition of non-aeration. Therefore, an intercept occurs since the normal drag force exerted on particles due to filtrate flow, F_n, is not trivial in such a condition.

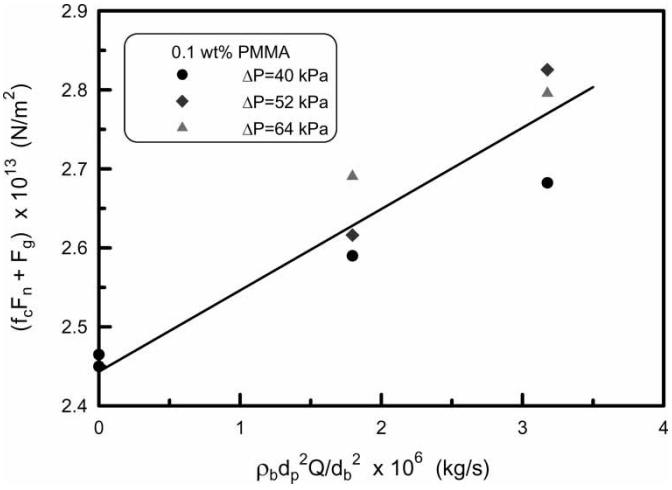

Figure 12. A plot of $(f_c F_n + F_g)$ versus $\rho_b d_p^2 Q / d_b^2$.

Once the empirical coefficients of the proposed models are obtained, the filtration flux at pseudo-steady state can be estimated by solving Eqs. (1) and (11) simultaneously. Figure 13 shows a comparison of pseudo-steady filtration flux between the calculated results and experimental data under various conditions. The diagonal line in this figure indicates the agreement between the calculated

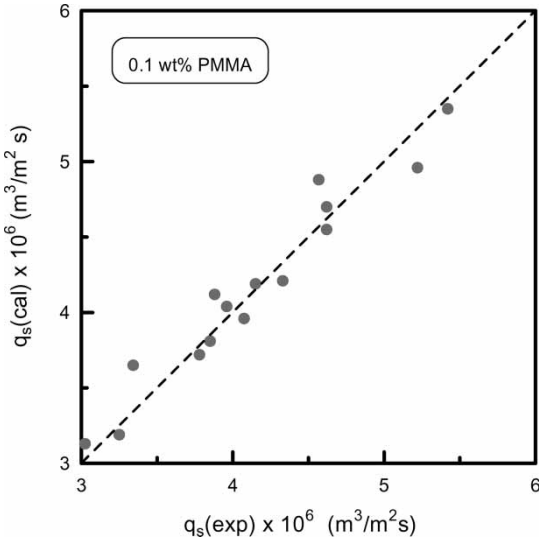

Figure 13. A comparison of pseudo-steady filtration flux between calculated results and experimental data.

results and the experimental data. Although the filtration fluxes are obtained under various filtration pressures and air flow rates, the deviations between these data are less than 9%. Since this result is quite reasonable and acceptable, the reliability and accuracy of the proposed models are demonstrated.

CONCLUSIONS

A force balance model for particle deposition on the membrane surface was derived based on hydrodynamics. The pseudo-steady filtration flux could be estimated by solving this theoretical model and basic filtration equation simultaneously. The deviations between calculated results and experimental data are less than 9%. The effects of operating conditions, such as aeration intensity and filtration pressure, on the filtration flux, membrane blocking, and the cake properties in submerged membrane filtration have been discussed thoroughly. The filtration resistances due to cake formation and membrane blocking played significant roles in determining the overall filtration resistance, the membrane blocking and cake formation contributed 50–80% and 10–30%, respectively, to the overall filtration resistance. A 75% decrease in cake resistance could be obtained when the air flow rate increased from 0 to 3.33×10^{-4} m^3/s. Consequently, an increase in aeration intensity led the filtration flux to be increased. Furthermore, a higher filtration pressure caused more severe membrane blocking and then to lower filtration flux. The cake properties and the filtration resistance caused by the membrane internal blocking were analyzed and could be regressed to empirical functions of the filtration pressure.

NOTATIONS

C_1 correction factor defined in Eq. (2) (−)
C_2 a factor defined in Eq. (5) (−)
C_3 a coefficient used in Eq. (7) (−)
C_4 correction factor defined in Eq. (9) (−)
C_D drag coefficient (−)
d diameter (m)
E_o the Eotvos number ($Eo \equiv g\rho_l d_b^2/\sigma$) (−)
F_g gravitational force of particles (N)
F_n drag force exerted on particles in the filtration direction (N)
F_t tangential drag force exerted on particles (N)
f_c friction coefficient between particles (−)
f_r bubble frequency (s^{-1})
g gravitational acceleration (m/s^2)
L_c cake thickness (m)
L_m thickness of porous medium (m)
M_o the Morton number ($Mo \equiv g\mu_l^4/\rho_l\sigma^3$) (−)

ΔP filtration pressure (N/m^2)
Q volumetric flow rate of air (m^3/s)
q filtration rate (m^3/m^2 s)
q_s filtration rate at the pseudo-steady state (m^3/m^2 s)
R_c resistance of the filter cake (m^{-1})
Re_b the bubble Reynolds number ($Re_b \equiv \rho_l d_b u_b/\mu_l$) (−)
R_{if} resistance due to internal fouling in the membrane (m^{-1})
R_m resistance of the filter membrane (m^{-1})
R_t overall filtration resistance (m^{-1})
u velocity (m/s)
V volume (m^3)
w_c mass of dry cake per unit area (kg/m^2)

Greek Letters

α specific filtration resistance of cake (m/kg)
ε cake porosity (−)
μ viscosity of liquid (kg/s m)
ρ density (kg/m^3)
σ surface tension (N/m)
τ_b shear stress acting on the bubble surface (N/m^2)
τ_w shear stress acting on the membrane surface (N/m^2)

Subscripts

av average property
b bubble
l liquid
p particle

ACKNOWLEDGEMENTS

The authors wish to express their sincere gratitude to the National Science Council of the Republic of China for its financial support.

REFERENCES

1. Ueda, T., Hata, K., Kikuoka, Y., and Seino, O. (1997) Effects of aeration on suction pressure in a submerged membrane bioreactor. *Water Res.*, 31: 489–494.

2. Chen, V., Fane, A.G., Madaeni, S., and Wenten, I.G. (1997) Particle deposition during membrane filtration of colloids: Transition between concentration polarization and cake formation. *J. Membr. Sci.*, 125: 109–122.
3. Kwon, D.Y. and Vigneswaran, S. (1998) Influence of particle size and surface charge on critical flux of crossflow microfiltration. *Water Sci. Technol.*, 38: 481–488.
4. Bouhabila, E.H., Ben Aim, R., and Buisson, H. (1998) Microfiltration of activated sludge using submerged membrane with air bubbling: Application to wastewater treatment. *Desalination*, 118: 315–322.
5. Liu, R., Huang, X., Wang, C., Chen, L., and Qian, Y. (2000) Study on hydraulic characteristics in a submerged membrane bioreactor process. *Process Biochem.*, 36: 249–254.
6. Shim, J.K., Yoo, I., and Lee, Y.M. (2002) Design and operation considerations for wastewater treatment using a flat submerged membrane bioreactor. *Process Biochem.*, 38: 279–285.
7. Chang, S. and Fane, A.G. (2001) The effect of fiber diameter on filtration and flux distribution-relevance to submerged hollow fiber modules. *J. Membr Sci.*, 184: 221–231.
8. Kim, J.H. and DiGiano, F.A. (2006) Defining critical flux in submerged membranes: Influence of length-distributed flux. *J. Membr Sci.*, 280: 752–761.
9. Kim, J.H. and DiGiano, F.A. (2006) Particle fouling in submerged microfiltration membranes: Effects of hollow-fiber length and aeration rate. *J. Water Supply: Research Technol. Aqua.*, 55 (7–8): 535–547.
10. Liu, C.Z., Guo, C., Wang, Y.C., and Ouyang, F. (2003) Comparison of various bioreactors on growth and artemisinin biosynthesis of artemisia annual shoot cultures. *Process Biochem.*, 39: 45–49.
11. Choo, K.H. and Lee, C.H. (1998) Hydrodynamic behavior of aerobic biosolids during crossflow filtration in the membrane anaerobic bioreactor. *Water Res.*, 32: 3387–3397.
12. Lee, W., Kang, S., and Shin, H.S. (2003) Sludge characteristics and their contribution to microfiltration in submerged membrane bioreactors. *J. Membr. Sci.*, 216: 217–227.
13. Bouhabila, E.H., Ben Aim, R., and Buisson, H. (2001) Fouling characterisation in membrane bioreactors. *Separ. Purif. Technol.*, 22–23: 123–132.
14. Belfort, G., Davis, R.H., and Zydney, A.L. (1994) The behavior of suspensions and macromolecular solutions in crossflow microfiltration. *J. Membr. Sci.*, 96: 1–58.
15. Cui, Z.F., Chang, S., and Fane, A.G. (2003) The use of gas bubbling to enhance membrane process. *J. Membr. Sci.*, 221: 1–35.
16. Cheryan, M. (1998) *Ultrafiltration and Microfiltration Handbook*; Technomic Publishing Co.: Pennsylvania, USA, pp. 113–130.
17. Lu, W.M. and Hwang, K.J. (1995) Cake formation in 2-D cross-flow filtration. *A.I.Ch.E. J.*, 41: 1443–1455.
18. Hwang, K.J. and Lin, K.P. (2002) Cross-flow microfiltration of dual-sized submicron particles. *Sep. Sci. Technol.*, 37: 2231–2249.
19. Lu, W.M. and Ju, S.C. (1989) Selective particle deposition in cross-flow filtration. *Sep. Sci. Technol.*, 24: 517–540.
20. Hermia, J. (1982) Constant pressure blocking filtration law: Application to power-law non-Newtonian fluid. *Trans. Inst. Chem. Eng.*, 60: 183–187.
21. Ho, C.C. and Zydney, A.L. (2000) A combined pore blockage and cake filtration model for protein fouling during microfiltration. *J. Colloid Interface Sci.*, 232: 389–399.

22. Fan, L.S. and Tsuchiya, K. (1990) *Bubble Wake Dynamics in Liquids and Liquid-Solid Suspensions*; Butterworth-Heinemann: Stoneham, MA, USA, pp. 17–69, Chap. 2.
23. Sherwood, J.D. (1988) The force on a sphere pulled away from a permeable half-space. *Physicochem. Hydrodyn.*, 10: 3–12.
24. Tiller, F.M., Cramp, J.R., and Ville, F. (1980) A revised approach to the theory of cake filtration. In *Fine Particles Processing*; Sanasundaran, P. (ed.); Amer. Inst. Min. Met. Petr. Eng.: New York, USA; Vol. 2, pp. 1549–1558.
25. Wilkes, J.O. (2006) *Fluid Mechanics for Chemical Engineers*; Prentice Hall: New Jersey, USA, pp. 531–536, Chap. 10.
26. Hwang, K.J., Chou, F.Y., and Tung, K.L. (2006) Effects of operation conditions on the performance of cross-flow microfiltration of fine particle/protein binary suspension. *J. Membr. Sci.*, 274: 183–191.